J Solid State Electrochem (2006) 10: 389–396
DOI 10.1007/s10008-005-0004-z

ORIGINAL PAPER

S. Franger · S. Bach · J. P. Pereira-Ramos · N. Baffier

Partially substituted lithium manganese oxides as 3 V cathode materials for secondary lithium batteries

Received: 27 March 2005 / Revised: 11 April 2005 / Accepted: 2 May 2005 / Published online: 15 July 2005

Abstract Low temperature synthesis and electrochemical properties of partially substituted lithium manganese oxides are reported. We demonstrate various metallic cations (Cu^{2+}, Ni^{2+}, Fe^{3+}, Co^{3+}) can be incorporated in the 3 V layered cathodic material $Li_{0.45}MnO_{2.1}$. New compounds $Li_{0.45}Mn_{0.88}Fe_{0.12}O_{2.1}$, $Li_{0.45}Mn_{0.84}Ni_{0.16}O_{2.05}$, $Li_{0.45}Mn_{0.79}Cu_{0.21}O_{2.3}$, $Li_{0.45}Mn_{0.85}Co_{0.15}O_{2.3}$ are prepared. These 3 V cathode materials are characterized by the same shape of discharge-charge profiles but different values of the specific capacity, between 90 mAh g^{-1} and 180 mAh g^{-1}. The best results in terms of capacity and cycle life are obtained with the selected content of 0.15 Co per mole of oxide, as the optimum composition. The high kinetics of Li^+ transport in $Li_{0.45}Mn_{0.85}Co_{0.15}O_{2.3}$ compared to that in the Co-free material is consistent with a substitution of Mn(III) by Co(III) in MnO_2 sheets.

Keywords Lithium batteries · Soft chemistry · Manganese oxides · Partial substitution

Introduction

A drive to develop inexpensive and environmentally benign cathodes for rechargeable lithium batteries has generated intensive worldwide activity on manganese oxides. The manganese oxides have, however, been plagued by two major difficulties: (1) the lattice distortion (Jahn-Teller) associated with the widely pursued $LiMn_2O_4$ spinel oxides and (2) the dissolution of manganese into the electrolyte, particularly at high voltages. The main strategy for improving the cycling stability of the spinel compounds is to add heteroatoms such as Co, Al, Cr and Li to alleviate the Jahn-Teller effect, which is believed to be one of the reasons for cycling instability [1–3]. Conversely, this strategy has been little applied to improve the cycling properties of layered phases. Moreover, in spite of the interest of $LiMn_2O_4$, only a few works have been devoted to 3 V lithium manganese oxides.

The conventional solid state route [4, 5], as well as low temperature techniques [6, 7], allow to synthesize electrochemically active lithiated phases. Depending on the synthesis way, orthorhombic [4], mixture of $\beta/\gamma-MnO_2$ [5], monoclinic [6] and hexagonal [7] phases are obtained. Recently, a new lithium manganese oxide $Li_{0.45}MnO_{2.1}$, synthesized through an ion-exchange procedure from the sol–gel layered compound $Na_{0.45}MnO_{2+\delta}{\cdot}0.6H_2O$, has been investigated in our group [7]. It comes out that it constitutes an attractive material as 3 V cathode. We have moreover already proved that a partial cobalt substitution in the sol–gel birnessite, $Mn_{1-x}Co_xO_{1.84}{\cdot}0.6H_2O$, could improve the electrochemical performance of this manganese oxide, especially in terms of cycle life [8].

Thus, in this paper, we report the cobalt incorporation in the lithiated oxide $Li_{0.45}MnO_{2.1}$ and its effect on the electrochemical properties. Herein, we focus on the optimization of the cobalt content in the substituted material. For that purpose, a wide range of Co-based lithiated oxides has been synthesized and electrochemically tested. Attempts for changing cobalt against other cationic species have been also undertaken. The effect of other substituting elements including divalent (Ni^{2+}, Cu^{2+}) and trivalent cations (Al^{3+}, Cr^{3+}, Fe^{3+}, Bi^{3+}) on electrochemical performance of the lithium manganese oxides was also examined.

S. Franger · S. Bach (✉) · J. P. Pereira-Ramos
Laboratoire d'Electrochimie,
Catalyse et Synthèse Organique,
UMR CNRS 7582, ISCSA,
2 rue Henri-Dunant, 94320 Thiais, France
E-mail: bach@glvt-cnrs.fr
Tel.: +33-1-49781163
Fax: +33-1-49781323

N. Baffier
Laboratoire de Chimie Appliquée de l'Etat Solide,
UMR CNRS 7574, ENSCP, 11 rue Pierre et Marie Curie,
75231 Paris Cedex 05, France

Present address: S. Franger
LPCES, UMR CNRS 8648, ICMMO,
Université Paris XI, 91405 Orsay Cedex, France

Experimental

Synthesis

The starting material is the sol–gel layered compound $Na_{0.45}MnO_2{\cdot}0.6H_2O$ (its synthesis has been already reported in details, in ref. [7]). It exhibits an hexagonal symmetry with the following lattice parameters (SG: $P-3m1$), $a = 2.84$ Å, $c = 14.54$ Å. A quantitative ionic exchange reaction was carried out by refluxing $Na_{0.45}MnO_2{\cdot}0.6H_2O$, for 2 days, at 180 °C, in an aqueous solution containing a large excess of lithium hydroxide (LiOH, 1 mol L^{-1}) (which requires the use of a PTFE vessel) with or without a metallic cation (Me = Cr^{3+}, Fe^{3+}, Co^{2+}, Ni^{2+}... from acetate or nitrate salts, all obtained from Fluka). After cooling to RT and filtration, the remaining solid was washed with de-ionized water and dried at 60 °C. The same water content than that found in $Na_{0.45}MnO_2{\cdot}0.6H_2O$ is observed in the lithiated oxide. The anhydrous final compound is obtained after a thermal treatment at 300 °C, during 10 h, and corresponds to the following general formula (from elemental analysis): $Li_{0.45}Mn_{1-y}Me_yO_{2+\delta}$ ($0.05 \le \delta \le 0.3$) with $0.1 < y \le 0.2$ for partially substituted materials.

Chemical and structural analysis

The average oxidation state, Z_{Mn}, of manganese in the sample was determined by the following procedure. The sample (˜100 mg) was added in 50 cm^3 of concentrated H_2SO_4 (commercial 96 vol% solution) + 50 cm^3 of de-ionized and de-aerated water, in presence of an excess of ferrous(II) ammonium sulfate (from Fluka), until complete dissolution. After cooling to 20–25 °C, the excess of ferrous(II) ammonium sulfate is potentiometrically titrated (WE : platinum wire, RE : $Hg|Hg_2SO_4$) with a fresh, home made, potassium permanganate solution. At the same time a blank is run, under identical conditions. Chemical composition of the compounds was made twice by elemental analysis [Inductively Coupled Plasma-Mass Spectroscopy (ICP-MS)] with an accuracy of ±5%. X-ray diffraction experiments (XRD) were performed with an Inel diffractometer, using the Cu K_α radiation ($\lambda = 1.54178$ Å). Concerning Rietveld measurement, the reliability factors for points with Bragg contributions for patterns are: *R*-factors: $R_{wp} = 3.16\%$ and $R_p = 4.61\%$; χ^2: 3.74 and DW-Stat: 0.6395.

Electrochemical measurements

The electrolyte used was 1 mol l^{-1} $LiClO_4$, dried under vacuum at 180 °C for 15 h, dissolved in propylene carbonate (PC) or in a 1/3 (volume ratio) mixture of ethylene carbonate (EC) and dimethylcarbonate (DMC) (all chemicals were obtained from Fluka). The working electrode (WE) consisted of a stainless steel grid (7-mm diameter, 0.2-mm thick.) with a geometric area of 1 cm^2 on which the cathode material was pressed (5 T/cm^2). The cathode was made of a mixture of active material (80 wt%), graphite (7.5 wt%), acetylene black (7.5 wt%) and PTFE as binder agent (5 wt%). Electrochemical studies were carried out in two-electrodes cells (Swagelok type), with a lithium metal disk (used both as reference and counter electrodes). Electrochemical measurements were made with a Mac Pile apparatus, except ac-impedance measurements that were performed in a classical three electrodes cell, following an experimental procedure detailed elsewhere [8].

Results and discussion

When the quantitative ionic exchange of sodium ions from $Na_{0.45}MnO_2{\cdot}0.6H_2O$ against lithium ions is performed in absence of any other cationic species, the heat-treatment at 300 °C, in air, of the compound as prepared leads to a new $Li_{0.45}MnO_{2.1}$ phase ($Z_{Mn} = 3.77$). Figure 1a clearly indicates this compound is actually a mixture of two phases. The diffraction lines, (*002*): $d = 4.92$ Å and (*101*): $d = 2.38$ Å, can be indexed on the basis of an hexagonal lattice of the birnessite type, with the following parameters: $a = 2.84$ Å, $c = 9.84$ Å, while the other diffraction peaks can be ascribed to a spinel phase with $a = 8.16$ Å. When the heating treatment is performed at higher temperatures, the ratio between hexagonal and cubic phases is decreasing (the hexagonal phase is no more stable at elevated temperatures, $T > 300$ °C). Indeed, at 600 °C, we only observe a single well-crystallized spinel phase with a lattice parameter close to that observed for the well known $LiMn_2O_4$ cubic phase: $a = 8.237$ Å (this latter value being obtained from Rietveld refinement, Fig. 1b). The approximate ratio between hexagonal and cubic phases, below 600 °C, can be estimated following this general procedure (Rietveld refinements are actually very difficult to perform for medium temperatures experiments due to low resolution of the XRD patterns):

1. The knowledge of the cubic phase parameter, *a*, (from XRD patterns) allows to determine the chemical formula of the spinel manganese oxide (according to ref. [9])
2. The theoretical XRD patterns of this phase can be then modeled using a crystallographic software (like CaRIne, for example)
3. The knowledge of the hexagonal phase parameters, *a* and *c*, (from XRD patterns) allows to model the theoretical XRD patterns expected for this phase (for which, the simple chemical formula MnO_2 is applied, since lithium ions only have a very low contribution in the intensities observed);
4. the simulation of the experimental XRD patterns, by adding a certain percentage of cubic and hexagonal theoretical diagrams, allows to estimate the ratio of each one.

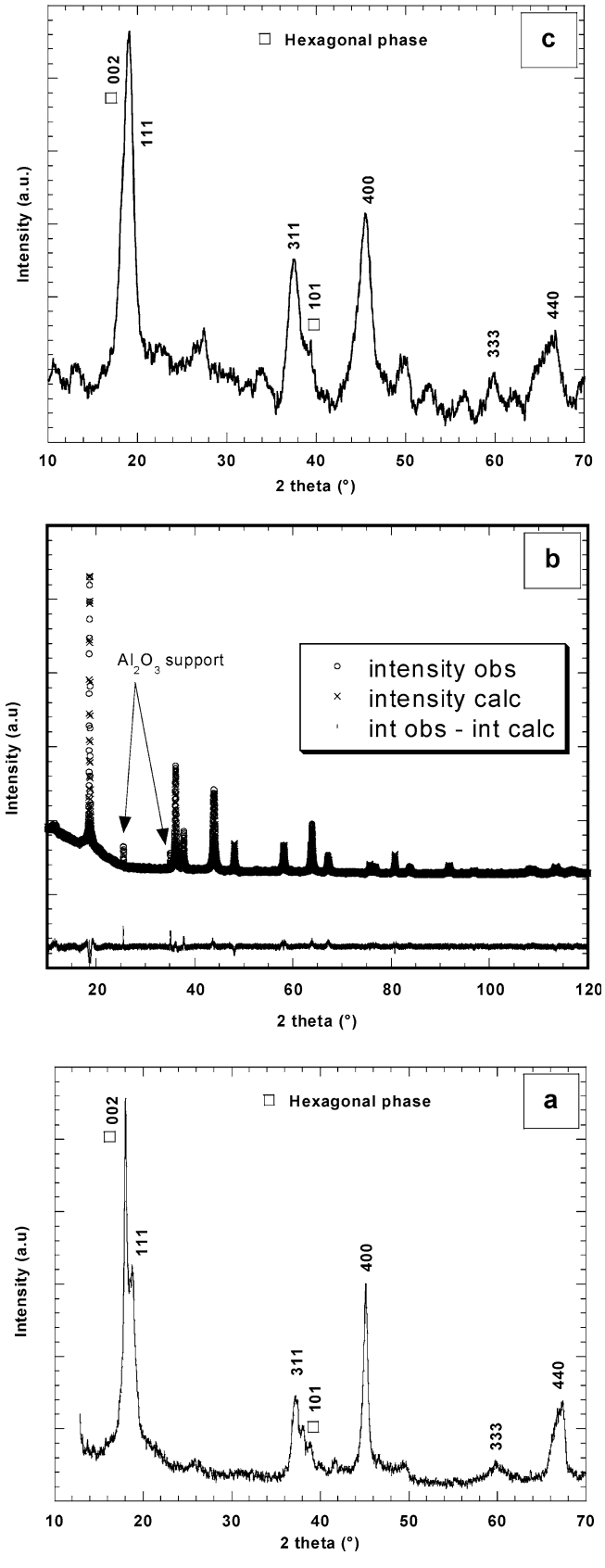

Fig. 1 Comparison of XRD diffraction patterns for **a** $Li_{0.45}MnO_{2+\delta}$ (300 °C/10 h), **b** $Li_{0.52}MnO_{2+\delta}$ (600 °C/10 h) (Rietveld refinement) and **c** $Li_{0.45}Mn_{0.85}Co_{0.15}O_{2+\delta}$ (300 °C/10 h)

The results obtained with this empirical method are presented in first part of Table 1.

Moreover, the determination of these ratio α and β, coupled with the chemical titration of the samples (giving the average oxidation state of manganese in the mixture), allows to determine the content of lithium ions into the layered hexagonal phase, according to

$$\alpha\%(Z_{\mathrm{Mn}})_{spinel} + \beta\%(Z_{\mathrm{Mn}})_{\mathrm{layered}} = (Z_{\mathrm{Mn}})_{\mathrm{mixture}}$$

One can then, with all these chemical formula and ratio for each phase, estimate the 'global' formula of the mixture. Results are summarized in Table 1.

The discharge–charge profile of the two-phases $Li_{0.45}MnO_{2.1}$ material (300 °C) is reported in Fig. 2. Almost 0.44 lithium ions are incorporated into the structure during the discharge (pseudo-plateau at 2.9 V). The charge process exhibits a well defined single step with 100% faradic efficiency. Moreover, for a cut-off voltage of 4.2 V, the faradic yield found is higher than that involved on discharge showing that a part of lithium ions (0.2 Li/mol), originally in the structure, can be removed below 4.2 V.

The pseudo-plateau at 2.9 V, as well as the small oxidation step up to 4 V (the latter being related to the lithium extraction from the 8a sites of the cubic structure), approach actually a spinel electrochemical behaviour, suggesting that probably both phases (layered and cubic) are involved in this electrochemical process. However, the shape of the galvanostatic curve progressively transforms, during cycling, into a more smooth "S"-type curve, corresponding to a pure layered material behaviour (solid solution of the Li–Mn–O system). This is probably due to the collapse of the spinel phase upon cycling, as previously mentioned (see Introduction).

The synthesis of $Li_{0.45}Mn_{1-y}Co_yO_{2+\delta}$ ($0.1 < y \leq 0.2$) is achieved by adding the stoichiometric amount of cobalt salt to the lithium hydroxide solution used during the exchange reaction. The heat-treatment at 300 °C, for 10 h, of the corresponding powders leads to the partially substituted lithiated phases, whose the chemical characteristics are summarized in Table 2.

All the diffraction peaks of $Li_{0.45}MnO_{2.1}$ are found again in the XRD pattern of the Co-based sample $Li_{0.45}Mn_{0.85}Co_{0.15}O_{2.3}$ (Fig. 1c). No additional phase such as a Co-rich phase appears, which is consistent with a probable substitution of Mn(III) by Co(III) ions in MnO_2 layers of both layered and cubic phases (we have indeed already demonstrated, thanks to Raman spectroscopy measurements performed onto birnessite-type materials [8, 10], that cobalt ions can be well incorporated into hexagonal layered structures and partial substitution of manganese by other heteroelements, in Li–Mn–O spinel systems, have also been widely reported in the literature). Moreover, after an heat treatment at 600 °C, as previously found for the pristine oxide, XRD analysis shows that a single spinel phase is obtained but, in this case, the linear decrease of the *a* parameter, in

Table 1 Estimation of the phases ratio in the new Li–Mn–O system

T (°C)	a_{spinel} (Å)	Spinel formula	Z_{Mn} spinel	a_{lay}(Å) c_{lay}(Å)	α	β	Z_{Mn} Lay.	Layered formula	"Mixture" formula
200	8.13	$Li_{0.8}MnO_{2.4}$	4	$a=2.8$ $c=5.0$	0.9	0.1	3.6	$Li_{0.37}MnO_2$	$Li_{0.45}MnO_{2.1}$
300	8.16	$Li_{0.7}MnO_{2.27}$	3.84	$a=2.8$ $c=4.9$	0.6	0.4	3.69	$Li_{0.3}MnO_2$	$Li_{0.45}MnO_{2.1}$
450	8.18	$Li_{0.65}MnO_{2.2}$	3.75	$a=2.8$ $c=4.8$	0.3	0.7	3.7	$Li_{0.15}MnO_2$	$Li_{0.5}MnO_{2.1}$
600	8.237	$Li_{0.52}MnO_{2.03}$	3.54	–	–	1	–	–	$Li_{0.52}MnO_{2.03}$

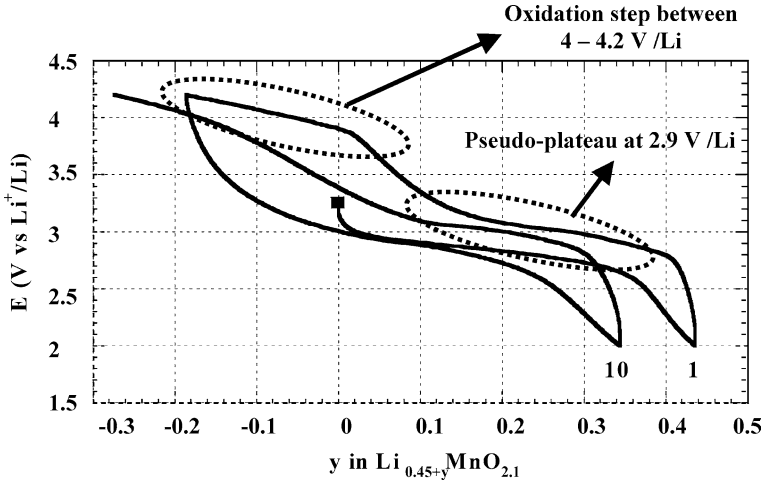

Fig. 2 Chronopotentiometric curves for the first and tenth reduction–oxidation cycles of $Li_{0.45}MnO_{2+\delta}$ at low current density (C/20 rate) in 1 mol L^{-1} $LiClO_4$/propylene carbonate

Table 2 Chemical composition of $Li_{0.45}Co_yMn_{1-y}O_{2+\delta}$after heat-treatment at 300°C

y (from elemental analysis) (±5%)	Mn(IV) content (%) (±2%)	δ value
$y=0.11$	73%	0.11
$y=0.13$	72%	0.13
$y=0.15$	68%	0.29
$y=0.17$	69%	0.33
$y=0.19$	74%	0.38

these spinel Co-based phases, with the cobalt content (Fig. 3), from 8.18 Å to 8.11 Å, mainly due to the lower size of Co^{3+}, clearly indicates the partial substitution of some Mn(III) by Co(III) in the cubic lattice.

The discharge–charge profiles of the two-phases $Li_{0.45}Mn_{1-y}Co_yO_{2+\delta}$ ($0.1 < y \leq 0.2$) oxides (300 °C) exhibit a shape (Fig. 4a) very close to that of Co-free oxide. Indeed, only one single reduction step between 3.5 V and 2 V typical of a layered MnO_2 phase is recorded. Once again, whatever the Co content, around 0.05 up to 0.1 Li ion can be extracted from the structure in the 4–4.2 V region. Both the additional oxidation process and the value of the faradic yield during the first insertion step strongly depend on the Co-content. Nevertheless, understanding of the role of cobalt upon electrochemical performance is difficult (Fig. 4b). Indeed, from their cycling behaviour examined at C/20 rate, it comes out that the lowest Co-contents (0.11–0.13) do not allow to stabilize the capacity around satisfactory values. The same trend is observed for the highest Co-content (0.19). In spite of a progressive

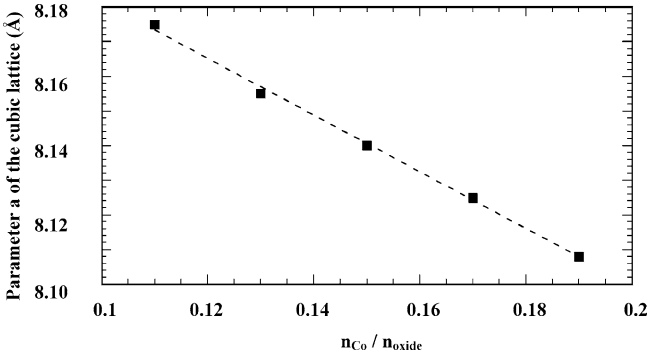

Fig. 3 Evolution of the cubic a parameter as a function of cobalt content, in the spinel unit cell of Co-based phases obtained after heat treatment, at 600 °C, for 10 h

improvement of the capacity with cycles, the specific capacity of $Li_{0.45}Mn_{0.83}Co_{0.17}O_{2.3}$ remains relatively low with 120 mAh g^{-1} after 20 cycles. Finally, the best result is achieved for the $Li_{0.45}Mn_{0.85}Co_{0.15}O_{2.3}$ compound with a specific capacity of 180 mAh g^{-1}.

In order to get some modification of the structure and electrochemical properties, the effect of various cations: Al^{3+}, Cr^{3+}, Fe^{3+}, Ni^{2+}, Cu^{2+}, Bi^{3+} has been also examined. The amount of metallic cations introduced during the ion exchange reaction has been adapted in order to ensure a theoretical value of 0.15 per mole of oxide. Two distinct sets of data are obtained. XRD patterns of samples heat-treated at 300 °C are recorded in Fig. 5a. In the case of aluminum, bismuth and chromium, besides the main diffraction lines expected for

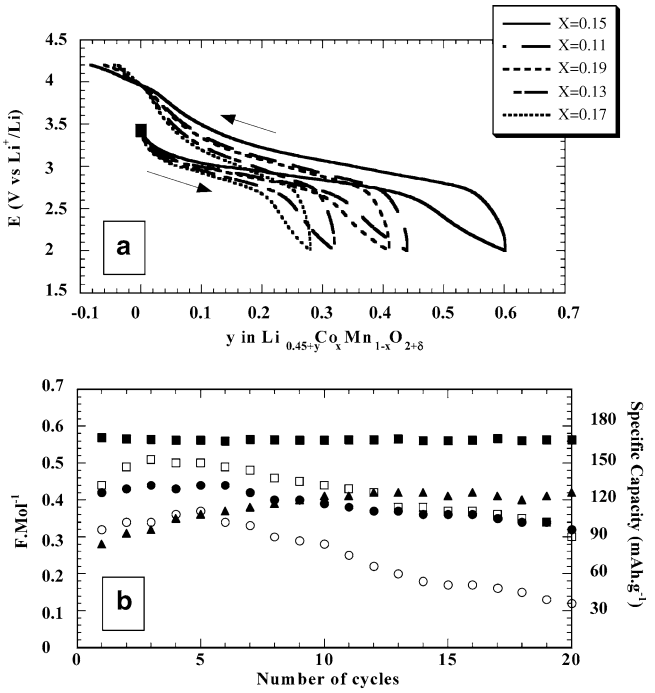

Fig. 4 Influence of the Co-content in $Li_{0.45}Mn_{1-y}Co_yO_{2+\delta}$ with $0.11 \leq y \leq 0.19$ **a** on the chronopotentiometric curves and **b** on the faradic yield (cycling limits 4.2–2.0 V, C/20) (*open square* $y = 0.11$; *open circle* $y = 0.13$; *filled square* $y = 0.15$; *filled triangle* $y = 0.17$; *filled circle* $y = 0.19$)

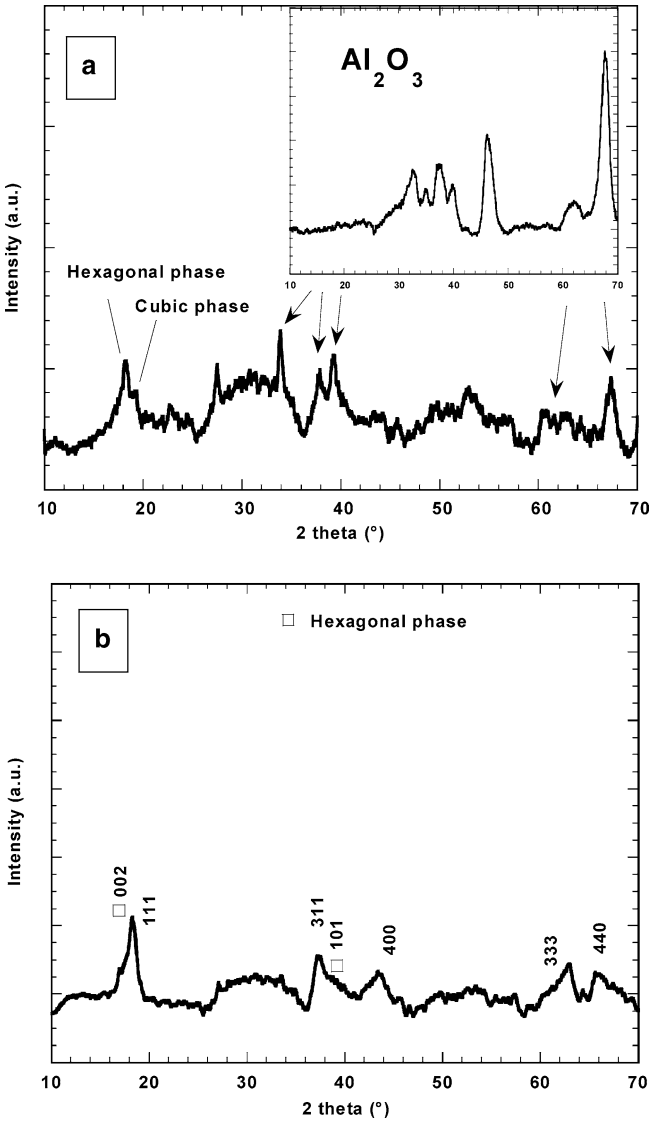

Fig. 5 **a** Typical X-Ray diffraction patterns in the case of aluminium substituted oxide; **b** X-Ray diffraction patterns of $Li_{0.45}Mn_{0.88}Fe_{0.12}O_{2.1}$ (similar patterns are observed for $Li_{0.45}Mn_{0.84}Ni_{0.16}O_{2.05}$ and $Li_{0.45}Mn_{0.79}Cu_{0.12}O_{2.09}$)

$Li_{0.45}MnO_{2.1}$, the presence of the corresponding thermodynamically stable oxides Al_2O_3, Bi_2O_3 and Cr_2O_3 is detected showing these cations do not enter the MnO_2 host lattice. Conversely, for iron, copper and nickel ions, it is evident from Fig. 5b that Fe^{3+}, Ni^{2+}, Cu^{2+} incorporate the structure of the manganese oxides, since only the fingerprint of the pristine $Li_{0.45}MnO_{2.1}$ system appears. However, the low intensity of the diffraction lines indicates disordered phases. Analysis of diffraction lines shows the appearance of two phases, a layered one with an hexagonal symmetry close to that described by Brec [11] and a spinel phase.

Table 3 summarizes the chemical data of the different partially substituted lithiated oxides. It can be seen that the presence of Fe^{3+}, Ni^{2+}, Cu^{2+} does not affect the quantitative Na/Li ion exchange reaction. Substitution is more efficient with divalent cations with $0.16Ni^{2+}$ and $0.21Cu^{2+}$ per mole of oxide but the presence of Fe^{3+} ions ensures a higher oxidation state of Mn. The iron content reached here, 0.12/mol is very close to the cobalt amount in the best Co(III) substituted material. The typical discharge–charge profiles of $Li_{0.45}Mn_{0.88}Fe_{0.12}O_{2.1}$ $Li_{0.45}Mn_{0.84}Ni_{016}O_{2.05}$ $Li_{0.45}Mn_{0.79}Cu_{0.21}O_{2.3}$ at C/20 rate are reported (Fig. 6).

The shape of the chronopotentiometric curves for the Co-free and Co-based forms is recovered : the working potential slowly decreases in one single step located near 2.9 V while the oxidation reaction is quantitative and allows a further extraction of lithium at high potential which never exceeds 0.1 Li per mole of oxide. Of interest

Table 3 Chemical composition of Fe, Ni and Cu-based $Li_yMn_{1-x}M_xO_{2+\delta}$ after heat-treatment at 300°C

Chemical composition	x (from elemental analysis) (±5%)	y (from elemental analysis) (±5%)	Mn(IV) content (%) (± 2%)	δ value
$Li_xFe_yMn_{1-y}O_{2+\delta}$	0.44	0.12	40%	0.10
$Li_xNi_yMn_{1-y}O_{2+\delta}$	0.45	0.16	33%	0.05
$Li_xCu_yMn_{1-y}O_{2+\delta}$	0.45	0.21	31%	0.09

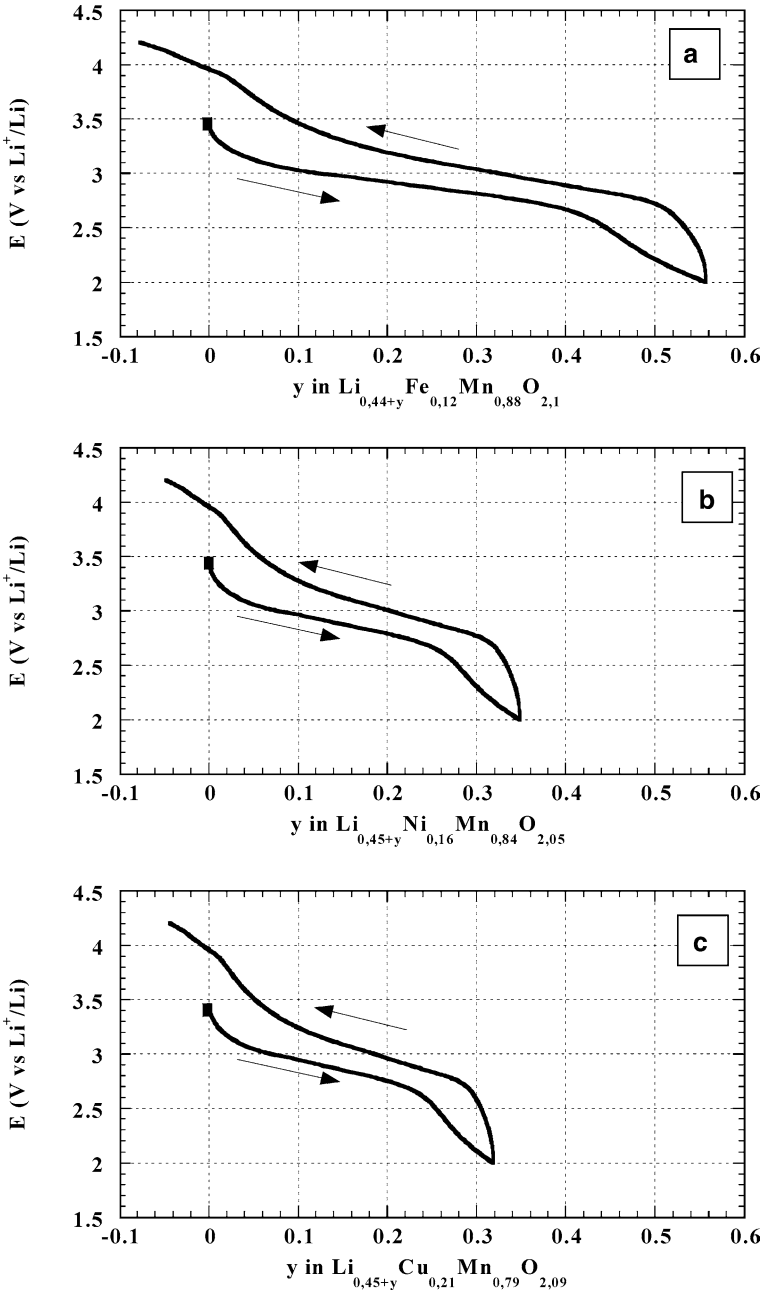

Fig. 6 Chronopotentiometric curves for the first reduction–oxidation cycle of **a** $Li_{0.45}Mn_{0.88}Fe_{0.12}O_{2.1}$, **b** $Li_{0.45}Mn_{0.84}Ni_{0.16}O_{2.05}$ and **c** $Li_{0.45}Mn_{0.79}Cu_{0.12}O_{2.09}$ at low current density (C/20 rate) in 1 mol.L^{-1} $LiClO_4$/propylene carbonate

is the small hysteresis between charge and discharge potentials.

The iron-based oxide is of interest with 0.55 F/mol in the first discharge, the Li uptake in nickel and copper-based materials being much lower around 0.3 F/mol. An evaluation of their cycling life was performed in the voltage range 4.2–2.0 V at C/20. Figure 7 outlines stable capacities for all the compounds. The discharge capacity decreases very early for the Fe-containing compound and, once again, after ten cycles to reach the value exhibited with divalent cations, i.e. around 100 mAh g^{-1}. The larger faradic yield found for the Fe-based compound in comparison with that expected from the Mn(IV) content as well as the early decrease of discharge capacity suggest ferric ions are probably involved in the reduction process leading then to Fe^{2+} and a behaviour similar to that offered with divalent cations.

Among all the doped manganese oxides studied here, it comes out that the Co-based material with the composition is the most promising. We have searched to evaluate the kinetics of Li transport in the compound by using ac-impedance spectroscopy. Surprisingly, EIS experiments give evidence for the formation of a surface layer on the electrode as soon as the material is reduced [12]. The formation of this surface layer takes place only when propylene carbonate is used as solvent or co-solvent. Therefore, 1 M $LiClO_4$ EC/DMC (1/3 by volume) electrolyte was used for EIS study, which allows to completely hinder the film formation. A typical impedance diagram obtained for $Li_{0.45}Mn_{0.85}Co_{0.15}O_{2.3}$.

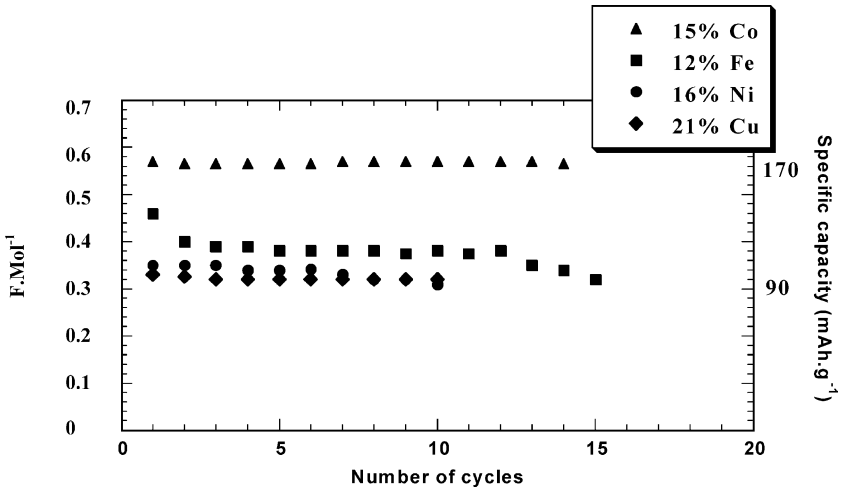

Fig. 7 Evolution of the specific capacity *vs* cycles number for the partially substituted lithiated oxides in $Li_{0.45}Mn_{0.85}Co_{0.15}O_{2.3}$, $Li_{0.45}Mn_{0.88}Fe_{0.12}O_{2.1}$, $Li_{0.45}Mn_{0.84}Ni_{0.16}O_{2.05}$ and $Li_{0.45}Mn_{0.79}Cu_{0.12}O_{2.09}$ (cycling limits 4.2–2.0 V, C/20)

(Fig. 8a) makes possible discrimination between the charge transfer semicircle at high frequency (f* = 100 Hz) and the Warburg region (3 Hz–0.3 Hz) corresponding to the 45 ° straight line (semi-infinite diffusion). Figure 8b observed for the reduced sample, $Li_{0.8}Mn_{0.85}Co_{0.15}O_{2.3}$ indicates qualitatively a slight shift of the frequency range for the Warburg region towards lower values and then a slower lithium diffusion kinetics can be expected. Moreover, these delimiting frequencies values of the semi-infinite diffusion region are slightly higher, in the Co-based oxides, than those achieved in the case of the parent oxide $Li_{0.45}MnO_{2.1}$, demonstrating the benefit of the partial Co-substitution for the enhancement of the lithium diffusion kinetics. Finally, we have to outline that the impedance diagram of the starting material $Li_{0.45}Mn_{0.85}Co_{0.15}O_{2.3}$ is completely

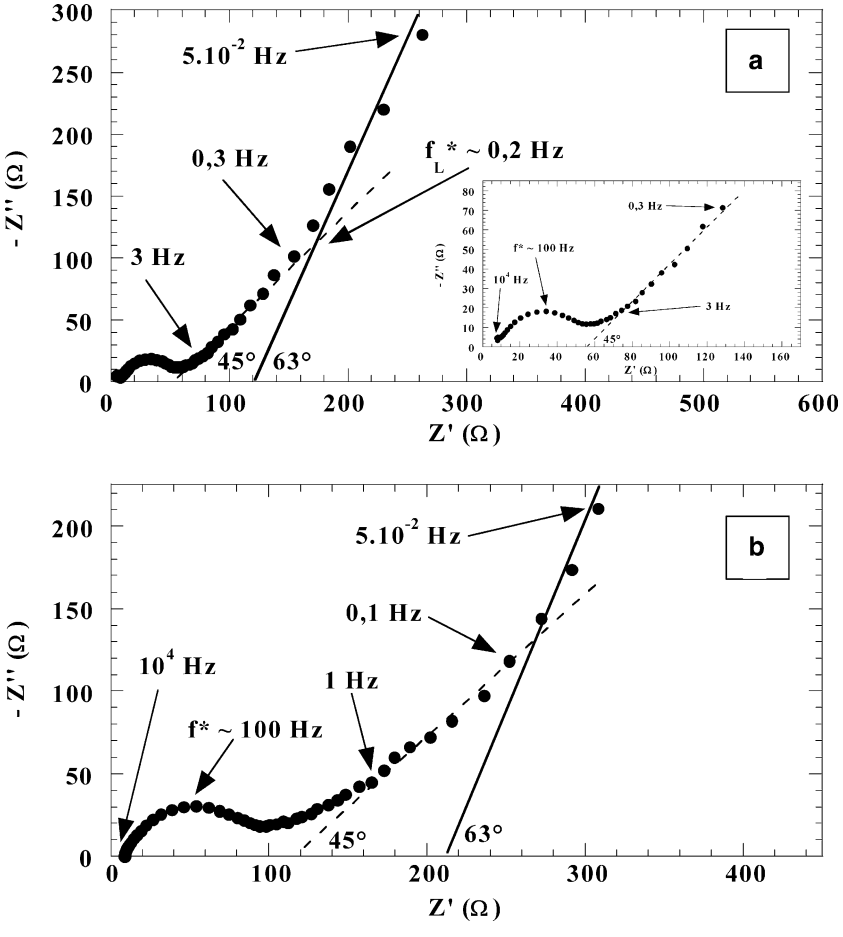

Fig. 8 ac-impedance diagrams of **a** $Li_{0.45}Mn_{0.85}Co_{0.15}O_{2.3}$ and **b** $Li_{0.8}Mn_{0.85}Co_{0.15}O_{2.3}$

recovered after oxidation of the reduced sample $Li_{0.8}Mn_{0.85}Co_{0.15}O_{2.3}$ showing the reversibility of the lithium insertion reaction, in the host lattice.

References

1. Tarascon JM, Wang E, Shokoohi FK, Mc. Kinnon WR, Colson S (1991) J Electrochem Soc 138:2859
2. Sigala C, Guyomard D, Verbaere A, Piffard Y, Tournoux M (1995) Solid State Ionics 81:167
3. Guoha L, Ikuta H, Uchida T, Wakihara M (1996) J Electrochem Soc 143:178
4. Yoshio M, Nakamura H, Xia Y (1999) Electrochim Acta 45:273
5. Levi E, Zinigrad E, Teller H, Levi MD, Aurbach D, Mengeritsky E, Elster E, Dan P, Granot E, Yamin H (1997) J Electrochem Soc 144:4133
6. Bruce PG, Armstrong AR, Gitzendanner RL (1999) J Mat Chem 9:193
7. Franger S, Bach S, Pereira-Ramos JP, Baffier N (2000) J Electrochem Soc 147:3226
8. Franger S, Bach S, Farcy J, Pereira-Ramos JP, Baffier N (2002) J Power Sources 109:262
9. Strobel P, Le Cras F, Seguin L, Anne M, Tarascon JM (1998) J Solid State Chem 135:132
10. Julien C, Massot M, Baddour-Hadjean R, Franger S, Bach S, Pereira-Ramos JP (2003) Solid State Ionics 159:345
11. Bordet-Le Guenne L, Deniard P, Biensan P, Siret C., Brec R (2000) J Mat Chem 10:2201
12. Franger S, Bach S, Pereira-Ramos JP, Baffier N (2003) Electrochim Acta 48:891